JOURNAL OF GEOPHYSICAL RESEARCH, VOL. 106, NO. A11, PAGES 24,493–24,504, NOVEMBER 1, 2001

Coexistence of ionospheric positive and negative storm phases under northern winter conditions: A case study

G. Lu, A. D. Richmond, R. G. Roble, and B. A. Emery

High Altitude Observatory, NCAR, Boulder, Colorado, USA

Abstract. The response of the thermosphere and ionosphere to the famous January 10, 1997, geomagnetic storm is simulated using the thermosphere-ionosphere-electrodynamics general circulation model with realistic, time-dependent distributions of ionospheric convection and auroral precipitation as inputs. The simulation results show a dominant positive storm phase of increased F layer electron density over much of the northern winter hemisphere, but a negative storm phase with reduced electron density at middle and low latitudes is also evident in the simulation. The coexistence of both positive and negative storm phases is a result of the complex dynamical and chemical interactions between charged particles and neutral gases. The impulsive magnetospheric energy inputs via auroral precipitation and Joule heating generate traveling atmospheric and ionospheric disturbances (TADs and TIDs) which propagate from the northern auroral zone to lower latitudes and penetrate well into the Southern Hemisphere. The simulation results demonstrate that positive storm phases are caused primarily by enhanced auroral precipitation over high latitudes and by TIDs at middle and low latitudes. Globally speaking, composition changes in terms of enhancements in the N_2/O ratio are mainly responsible for negative storm effects. However, although there is some correlation between increases in N_2/O and decreases in the F layer critical frequency f_oF_2 in the winter hemisphere during the storm main phase and early recovery phase, the overall changes in f_oF_2 are also determined by other processes, such as the ionization production associated with enhanced auroral precipitation and the variations associated with TIDs. In the low to middle-latitude region changes in f_oF_2 approximately anticorrelate with changes at the height of the F layer electron density peak (e.g., h_mF_2) at 70°W during the storm main phase as well as its early recovery phase. This is attributed in part to the relation that exists between meridional wind velocity and vertical shear of that velocity for aurorally produced TADs.

1. Introduction

Geomagnetic storms and substorms are a way for the magnetosphere to release excess energy. A majority of the magnetospheric energy is transmitted into the upper atmosphere at high latitudes through auroral particle precipitation and ionospheric plasma convection. Intense auroral particle precipitation ionizes the neutral gas; collisions of precipitating electrons and ions with neutrals heat the atmosphere; and collisions between neutrals and fast convecting ions produce Joule frictional heating. It is therefore not surprising that the high variability of storms and substorms often cause complex dynamical and chemical disturbances in the ionosphere and thermosphere.

The most observed ionospheric variables are the total electron content (TEC) and the increase or decrease of the F layer peak electron density NmF_2, which is referred to as a positive or negative storm phase, respectively. A strong seasonal dependence is found in storm responses [*Prölss*, 1977; *Rodger et al.*, 1989]. Negative storm phases tend to form during summer when the higher molecular density contributes to more rapid recombination between electrons and ions [*Rishbeth*, 1989; *Burns et al.*, 1991, 1995], whereas positive storm phases more frequently form under winter conditions. Ionospheric storm effects have a pronounced local time variation as storm surges tend to be most intense in the early morning sector [*Prölss*, 1993]. Local time and seasonal variations in ionospheric storm response are the consequence of neutral composition changes and their

Paper number 2001JA000003.
0148-0227/01/2001JA000003$09.00

subsequent transport by the global wind fields [*Prölss*, 1993; *Fuller-Rowell et al.*, 1997].

Over the past two decades, theoretical studies, especially numerical simulations based on first-principle physical models, have vastly improved our understanding of the behavior of the ionosphere and thermosphere in response to the intense energy input from the magnetosphere [e.g., *Rishbeth et al.*, 1987; *Roble et al.*, 1987; *Fuller-Rowell et al.*, 1994, 1996, 1997; *Burns et al.*, 1991, 1995; *Field et al.*, 1998]. While there are numerous papers addressing storm-related ionospheric/thermospheric phenomena, no specific studies have been reported on the presence of opposite storm phases in the same seasonal hemisphere. In this paper we present the simulation results of the ionospheric/thermospheric response to the well-known storm event on January 10, 1997 [e.g., *Fox et al.*, 1998, and references therein], using the thermosphere-ionosphere-electrodynamics general circulation model (TIE-GCM) [*Richmond et al.*, 1992]. By incorporating realistic time-dependent ionospheric convection and auroral precipitation as inputs, the TIE-GCM depicts an interesting storm effect, that is, the coexistence of both positive and negative storm phases in the northern middle to low-latitude region. We discuss the possible mechanisms associated with this peculiar storm phenomenon in light of the model simulation.

2. Results

2.1. Geophysical Conditions and Model Inputs

The solar wind and interplanetary magnetic field (IMF) conditions for the January 1997 storm have been discussed in detail by *Farrugia et al.* [1998]. Figure 1 shows the IMF B_z component and geophysical parameters for January 10, 1997. The magnetic cloud arrived at Earth at ~0500 UT as indicated by the sharp southward turning of the IMF B_z from ~5 to 10 nT. Shortly after that, *Dst* started to drop rapidly, marking the storm main phase. After ~0900 UT, B_z became less southward and turned northward at 2100 UT. Correspondingly, the *Dst* index flattened out and then gradually became less negative after ~1100 UT, an indication of the storm recovery phase. As indicated by the *AE* index, there were several substorms during the passage of the magnetic cloud. The *AE* index shown here was calculated from the X component magnetic perturbations observed by 68 stations located between 55 and 76 magnetic latitudes in the Northern and Southern Hemispheres. The most intense substorm of *AE* ~2000 nT and the temporal positive excursion in *Dst* near 1100 UT were both associated with the solar wind pressure impulse [*Lu et al.*, 1998a]. The bottom two panels show the distributions of the cross-polar-cap electric potential drop and the Joule heating rate derived using the assimilative mapping of ionospheric electrodynamics (AMIE) procedure [*Richmond and Kamide*, 1988].

The data inputs to AMIE for this event include ion drift and auroral precipitation measurements from three DMSP satellites, auroral precipitation observations from two NOAA spacecraft, global auroral UV images from the Polar satellite, ion drift measurements from six Super Dual Auroral Radar Network high-frequency radars and from the Millstone Hill and Sondrestrom incoherent scatter radars, and magnetic perturbations from 119 ground magnetometers (see *Lu et al.* [1998a] for more information). The cross-polar-cap potential drops varied from tens of kV during northward IMF to over 100 kV during southward IMF, with the strongest potential drop of 220 kV around 1100 UT. The hemispheric integrated Joule heating rate was well correlated with the *AE* index, with a correlation coefficient of 0.91 in the Northern Hemisphere and 0.76 in the Southern Hemisphere [*Lu et al.*, 1998a]. Large Joule heating dissipation rates were found during the early part of the storm between 0600 and 1200 UT. The Joule heating rate exceeded 500 GW around 0800 and 1100 UT, respectively. As discussed later in the paper, strong Joule heating was responsible for traveling ionospheric disturbances as shown by the TIE-GCM.

To model the ionospheric/thermospheric response to the storm, we used the 5-min resolution patterns of ionospheric convection and auroral precipitation derived from AMIE as inputs to the TIE-GCM, which was also run in a 5-min time step. In addition to the ionospheric inputs from AMIE, the TIE-GCM also incorporates the semidiurnal tides at the lower boundary [*Fesen et al.*, 1991] and solar EUV and UV fluxes (the F10.7 index was 72.9×10^{-22} W m^{-2} Hz^{-1} on January 10, 1997). The model has an effective 5° latitude by longitude geographic grid and 29 constant pressure levels extending approximately from 97 to 600 km in altitude. A reference quiet time background is obtained from a 24-hour model run using the same ionospheric inputs at 0000 UT on January 9 but fixed in local time and magnetic latitude as the Earth rotates. The O^+ flux specification at the TIE-GCM upper boundary remains unchanged from quiet time conditions throughout the storm. This may be an oversimplified upper boundary condition for the TIE-GCM as it is known that the plasma in the outer plasmasphere can vary dramatically during geomagnetic storms [e.g., *Gallagher et al.*, 2000]. The O^+ flux has a significant effect on NmF_2 (for instance, by reducing the downward O^+ flux at night from 6×10^8 to 3.5×10^8 cm^{-3} s^{-1}, the nightside NmF_2 is accordingly reduced by nearly 100%) but has very little effect on h_mF_2. For both quiet day and active day model runs shown in this study, the daytime O^+ flux was specified as 2.1×10^8 cm^{-2} s^{-1} and the nighttime O^+ flux was 3.5×10^8 cm^{-2} s^{-1}, both downward. Normally, the O^+ flux is upward during the day but was changed to be downward to match electron densities from the International Reference Ionosphere model [*Bilitza*, 1990] as discussed by *Fesen et al.* [2000]. The O^+ flux also varied as a function of magnetic latitude and

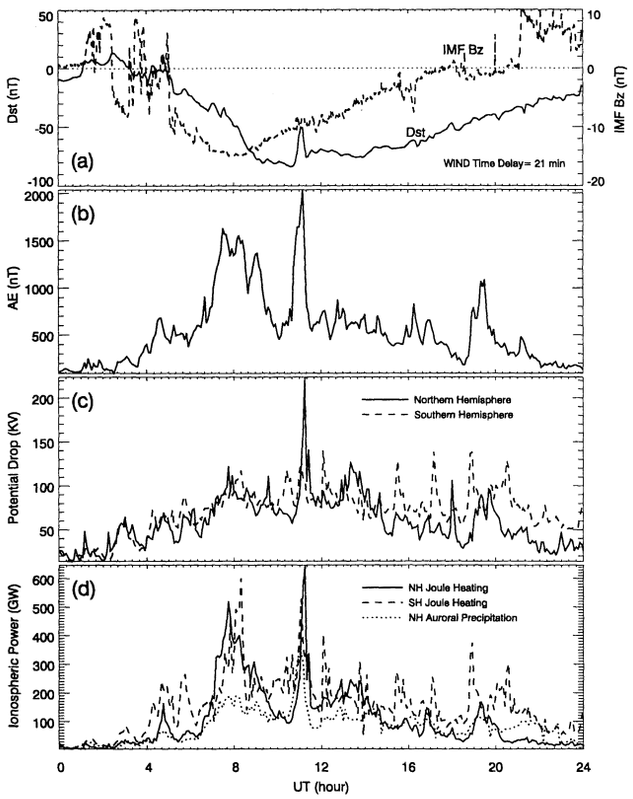

Figure 1. Distributions of (a) *Dst* and IMF B_z component, (b) the *AE* index, (c) the cross-polar-cap potential drop, and (d) the hemispheric integrated ionospheric Joule heating rate and auroral electron energy flux. A time delay of 21 min has been applied to the IMF data measured by Wind to account for the propagation from the satellite location to the magnetopause.

solar zenith angle, and linear interpolations between the daytime and nighttime values were made during sunrise and sunset between 80° and 100° zenith angles.

The January 1997 geomagnetic storm has been the subject of several papers regarding its thermospheric/ionospheric impacts. While only a moderate enhancement of ionospheric electric field and currents was reported over Scandinavia [e.g., *Schlegel and Collis*, 1999], a significant increase in electric field in excess of 100 mV m^{-1} was seen in Greenland during the storm [*Sanchez et al.*, 1998]. A daytime negative storm phase was observed with the Millstone Hill incoherent scatter (IS) radar on January 10 [*Mikhailov and Förster*, 1999] and was attributed to the decrease in the $O/(N_2+O_2)$ ratio. Furthermore, traveling atmospheric/ionospheric disturbances (TADs/TIDs) were evident through coordinated analysis of the data obtained by three IS radars (e.g., Sondrestrom, Millstone Hill, and Arecibo) which were found to be responsible for the F_2 layer fluctuations [*Buonsanto et al.*, 1999].

2.2. TEC Variations

Plate 1 shows a series of maps of the calculated TEC differences with respect to the quiet time background from 0600 to 2330 UT on January 10, 1997. Note that TEC calculated in the TIE-GCM is the height-integrated electron density from 97 km up to ~600 km (the altitude range of the model) so the contribution of higher altitude electrons to TEC has not been included. It is estimated that the electron column density above the TIE-GCM upper boundary amounts up to 25% of the TEC within the TIE-GCM altitude range in the high-latitude region (~80° geographic latitude) and 45% in the midlatitude region (~45° geographic latitude) and 100% near the equator [*Lu et al.*, 1998b]. Prior to the storm main phase at 0600 UT, TEC was only weakly increased by about 2 TECU (1 TECU = 10^{12} electrons cm^{-2}) over the auroral zone. During the storm, TEC increased dramatically in the auroral zone by more than 10 TECU in magnitude. After 1330 UT the enhancement of TEC in the auroral region gradually diminished until ~1900 UT when another moderate substorm took place. By the end of the day the *AE* index returned to its prestorm value and the auroral zone TEC enhancement became marginal again.

In addition to the TEC changes (primarily enhancements) over the auroral zone, there are middle- and low-latitude TEC changes that are more complex due to the presence of both TEC enhancement and depletion. An area of increased TEC first appeared in the midlatitude region near local noon. From 0800 to 1730 UT it not only intensified in magnitude but also expanded spatially. The area of enhanced TEC at middle latitudes moved westward and equatorward. By 1930 UT, however, the magnitude of TEC enhancement had been drastically reduced and was only seen at low latitudes. During the late UTs on the same day (January 10, 1997), TEC increased again at low latitudes in the prenoon sector, but the magnitude of TEC enhancement was substantially smaller than that at earlier hours. A region of decreased TEC evolved initially in the early morning just equatorward of the auroral zone after the onset of the first major substorm at ~0800 UT. As the storm progressed, the TEC depletion zone gradually moved toward dayside along with the rotation of the Earth. At 1730 UT a well-developed TEC depletion zone was found centered at ~55° geographic latitude near the local noon meridian. Thereafter the depletion zone remained in the postnoon sector and gradually disappeared locally, instead of moving into the nightside with the corotation. By the end of the day, TEC was nearly back to its background value at the dayside middle latitudes as well as in the polar region.

2.3. The f_oF_2 and N_2/O Variations

Figure 2 shows the difference maps of f_oF_2 in the northern winter hemisphere at selected times between 0800 and 2230 UT on January 10. The F layer critical frequency f_oF_2, which is directly related to the F layer peak electron density NmF_2 ($f_oF_2(Hz) = 9.0 \times \sqrt{NmF_2(m^{-3})}$), increased over the high-latitude auroral zone where the precipitation of keV electrons

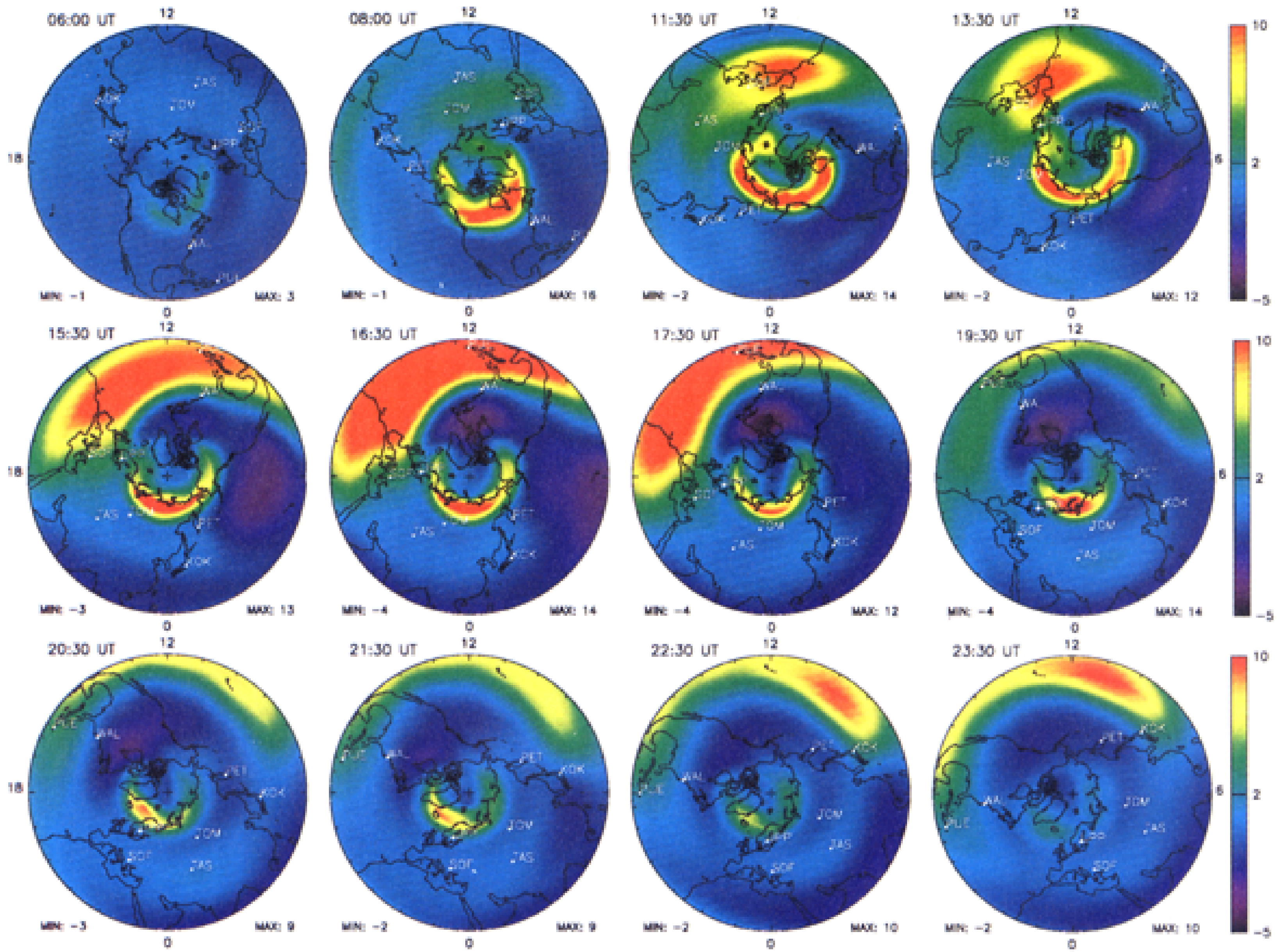
06:00 UT
08:00 UT
11:30 UT
13:30 UT
15:30 UT
16:30 UT
17:30 UT
19:30 UT
20:30 UT
21:30 UT
22:30 UT
23:30 UT
12
18
6
0
MIN: -1
MAX: 3
MIN: -1
MAX: 16
MIN: -2
MAX: 14
MIN: -2
MAX: 12
MIN: -3
MAX: 13
MIN: -4
MAX: 14
MIN: -4
MAX: 12
MIN: -4
MAX: 14
MIN: -3
MAX: 9
MIN: -2
MAX: 9
MIN: -2
MAX: 10
MIN: -2
MAX: 10
10
2
-5

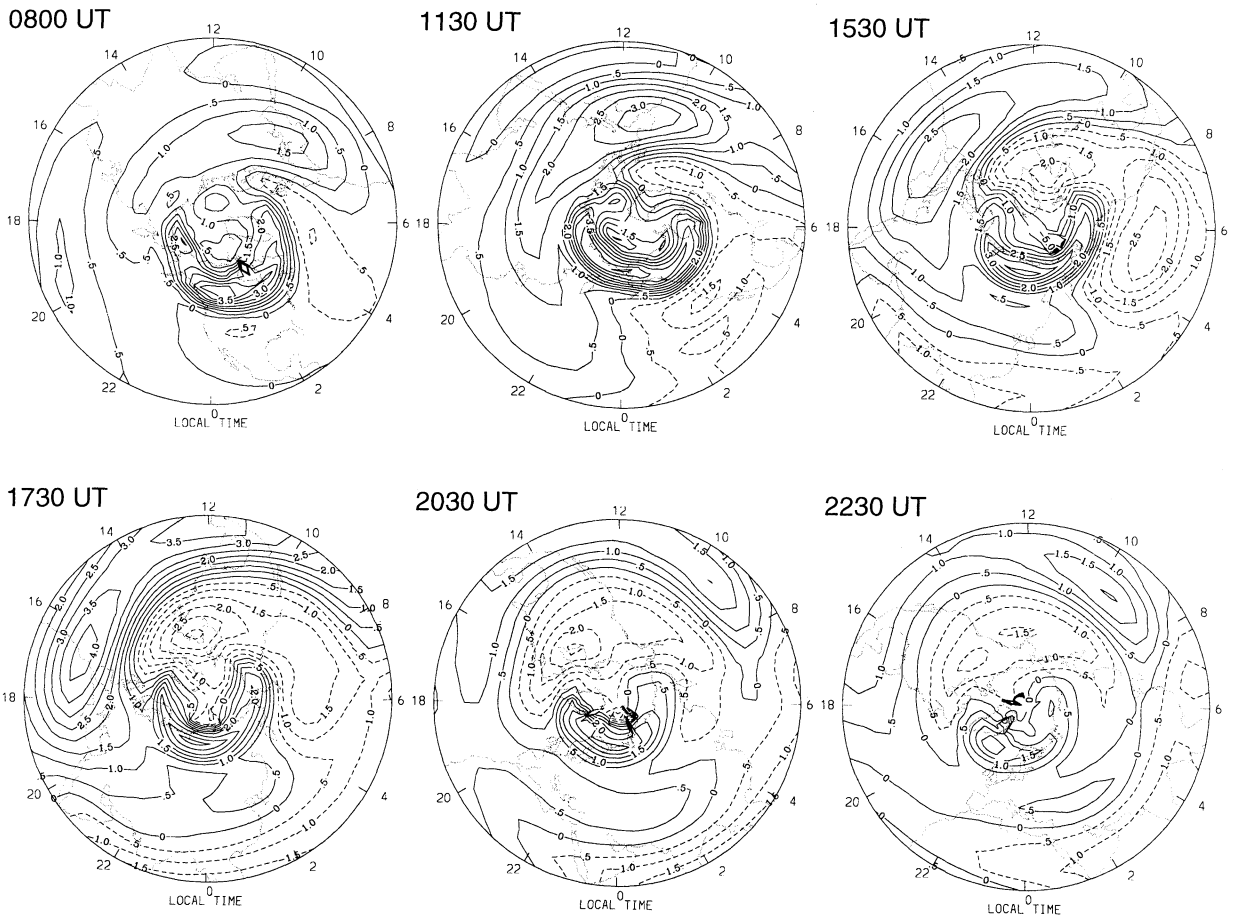

Figure 2. Changes in f_oF_2 with respect to the quiet time background between 0800 and 2230 UT. Solid and dashed contours represent increase and decrease in f_oF_2, respectively. The contour interval is 0.5 MHz.

and ions effectively help ionize the neutral gas at the F layer height. Equatorward of the auroral zone was a region of decreased f_oF_2; it first appeared in the early morning sector after the storm commencement and then slowly moved into the dayside. At middle to low latitudes there was another region of increased f_oF_2 but slightly smaller in magnitude compared to the auroral zone enhancements. Although TEC shown in Plate 1 is the integral of electron density from 97-600 km, we find that the distribution of f_oF_2 is closely related to the distribution of TEC, because the F layer electron density tends to dominate the TEC.

Figure 3 shows the difference maps of the ratio of N_2 to O number densities at the pressure level $ZP = 2$ (approximately 300 km altitude) at the same UT times as in Figure 2. At 0800 UT the increase in N_2/O was confined in the auroral zone, where enhanced auroral particle heating as well as Joule heating associated with strong substorm activity transport the molecular-rich air upward from the lower thermosphere. The peak of the N_2/O enhancement was located in the early morning sector. As time passed, the region of increased N_2/O expanded to lower latitudes where it gradually shifted to the dayside. The prevailing south-to-north circulation under the January solstice condition, however, prevented this molecular-rich air from propagating further equatorward. The change in N_2/O ratio peaked at ~50°N, with its equatorward edge extending to ~30°N. Although the N_2/O enhancement is the combination of an increase in N_2 and a decrease in O, the changes of N_2/O shown in Figure 3 are dominated by the changes in N_2. The changes in O_2 (not shown) were very similar to N_2.

Composition changes, particularly the increase of neutral molecular densities, are known as the main cause of negative storm phases [*Prölss*, 1987]. Indeed, a high

Plate 1. Maps of TEC changes with respect to the quiet time background between 0600 and 2330 UT on January 10, 1997. The maps are plotted above 15° geographic latitude, and the color scale is in TECU (1 TECU = 10^{12} electrons cm^{-2}).

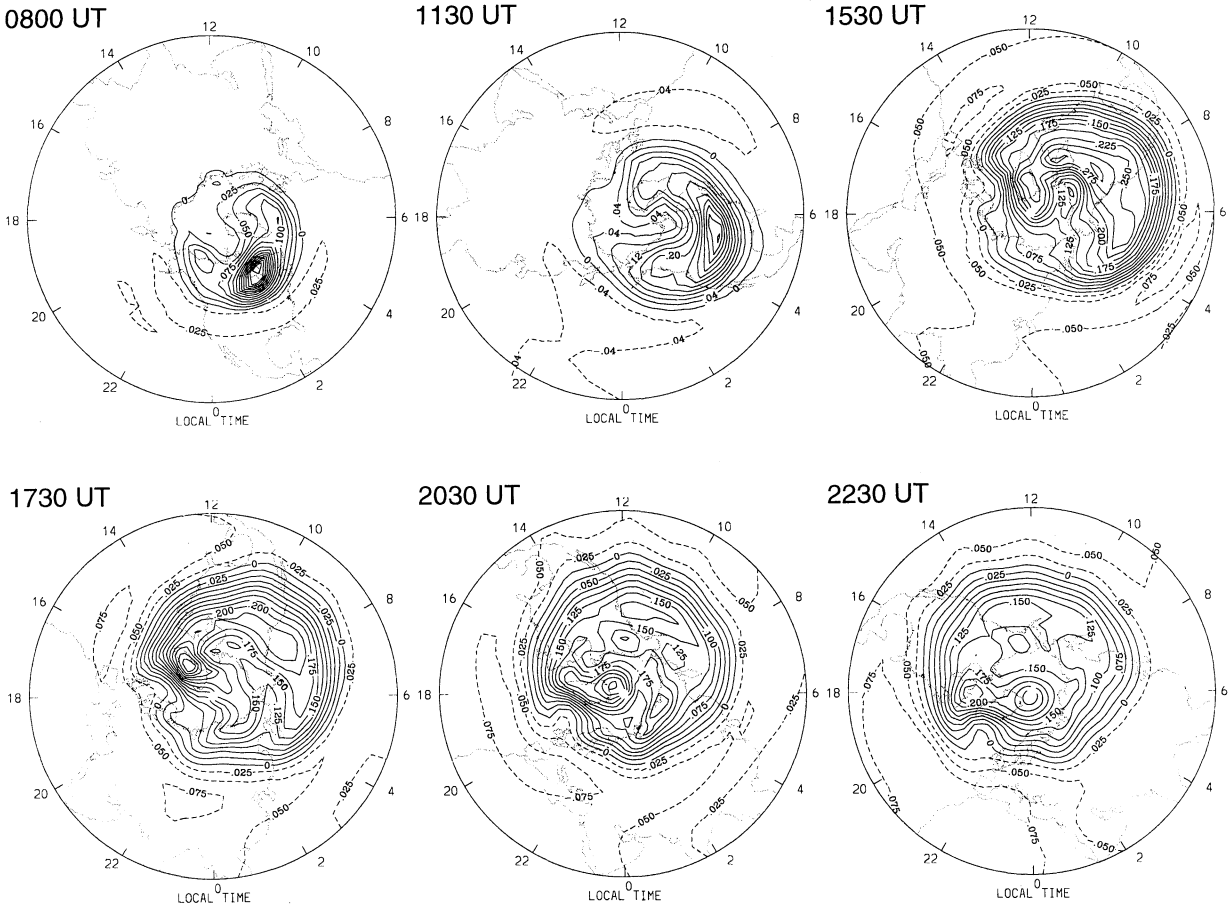

Figure 3. Similar to Figure 2, but for changes in the N_2/O ratio. Solid and dashed contours represent increase and decrease of N_2/O, respectively.

correlation between the region of enhanced molecular species in the neutral gas and the decrease of NmF_2 has been shown by *Fuller-Rowell et al.* [1997] based on the numerical simulation of an idealized geomagnetic storm. By comparing Figure 3 with Figure 2, the area of decreased f_oF_2 can be related approximately to the region where the N_2/O ratio increases. However, we note that there is not always a direct one-to-one anti-correlation between the two. For instance, at 1130 UT, just after an auroral intensification, the peak of N_2/O enhancement was at ~50°N and 0500 local time (LT), but the decrease in f_oF_2 was centered around ~40°N and 0400 LT. This offset between the N_2/O increase and the f_oF_2 decrease during the storm early recovery phase can be interpreted by the interplay between the production of electrons via ionization associated with auroral precipitation at high latitudes and the loss of electrons due to recombination fed by the N_2 (and O_2) density enhancement that spanned from high to middle latitudes. A better correlation between the N_2/O ratio increase and f_oF_2 decrease was seen during the late recovery phase (e.g., from 1730 to 2230 UT) when the enhancement in auroral precipitation had diminished.

2.4. NmF_2 Variations: Data-Model Comparison

Limited ionosonde measurements of NmF_2 were available in the Northern Hemisphere. Figure 4 shows the comparison of ionosonde data and model results at eight stations indicated in Plate 1. Unfortunately, there were no usable ionosonde data from the North American high-latitude region. In the American sector, the mid-latitude station Wallops Island observed a storm time NmF_2 value smaller than its monthly median during daytime, indicative of a negative storm phase. The modeled NmF_2 value at that location was also smaller than its corresponding quiet time background, but the daytime model results were nearly twice the observed values. At the low-latitude station in Puerto Rico, both the observations and the model showed a positive storm phase, that is, the storm time NmF_2 values were larger than the quiet time values. The modeled NmF_2 for both quiet time and storm time agreed reasonably well with the observations. In western Europe and over Russia, positive storm phases were evident in observations as well as in model results at middle and lower latitudes. In the Asian sector, there was not much of change in

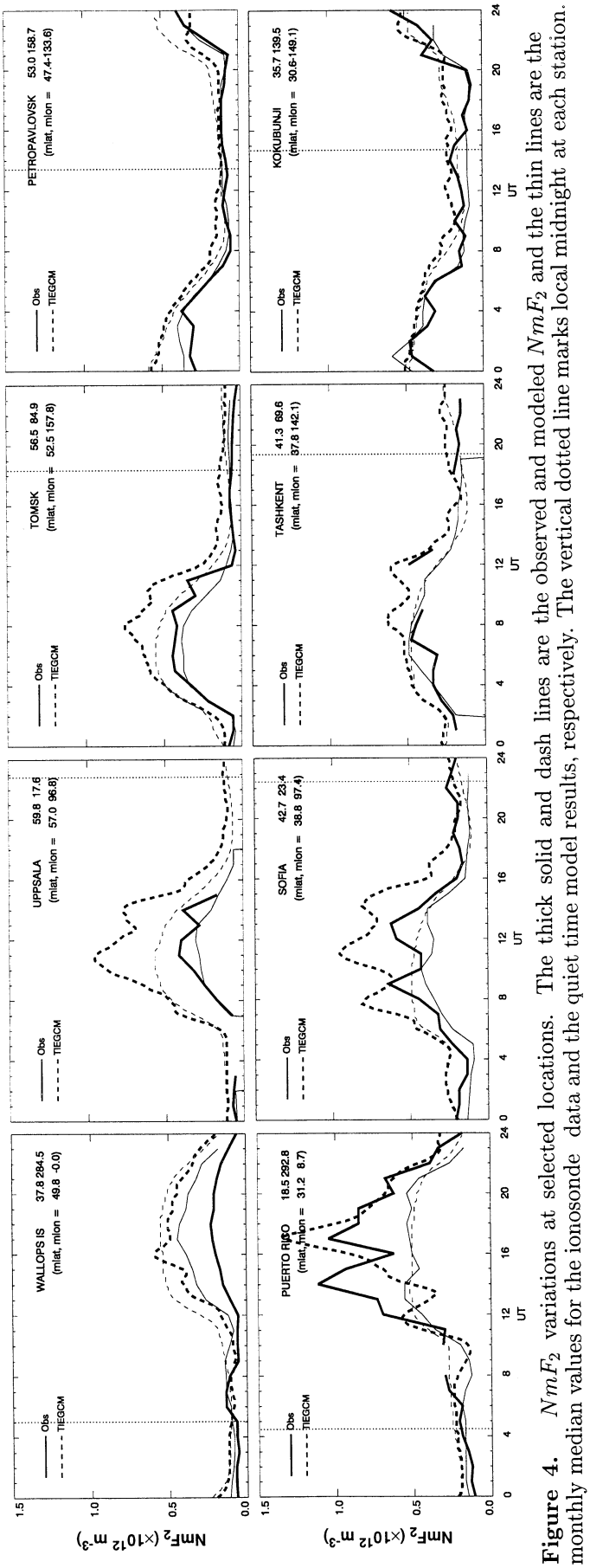

Figure 4. NmF_2 variations at selected locations. The thick solid and dash lines are the observed and modeled NmF_2 and the thin lines are the monthly median values for the ionosonde data and the quiet time model results, respectively. The vertical dotted line marks local midnight at each station.

NmF_2, indicating very little storm effect in that longitude sector.

Figure 4 demonstrates that the storm time ionospheric response is rather complicated, with both temporal and spatial variations. While the model results showed good qualitative agreement with the observations, the TIE-GCM overestimated NmF_2 in the northern midlatitude to high-latitude (above ~40°) regions. A possible cause of this overestimation is that the specified downward O^+ flux at the upper boundary of the model was too high, and the modeled T_n was too low as discussed by *Buonsanto et al.* [1999] when comparing with the neutral temperatures observed at Millstone Hill. Though not shown here, it is worth pointing out that the modeled NmF_2 was in much better quantitative agreement with the ionosonde data at low latitudes as well as in the summer Southern Hemisphere for this particular event.

2.5. Relation Among the Different Parameters

Figure 5 shows the difference plots of various fields with respect to the quiet time background at 70°W. The neutral meridional wind perturbations are shown in Figure 5a, where negative values (shown as dashed contours) represent southward perturbation winds. The arrows on the top and bottom of the panel correspond to the times of Joule heating peaks in the Northern and Southern Hemispheric auroral zones, respectively. The larger arrows represent Joule heating rates exceeding 500 GW. As shown in Figure 5a, TIDs as represented here by the meridional wind surges (highlighted by the heavy dashed lines) were launched by enhanced Joule heating in the northern auroral zone (~60° in geographic latitude or 70° in magnetic latitude); they propagated southward at a phase speed of ~750 m s^{-1} and penetrated deep into the Southern Hemisphere. Although there were similar enhanced Joule heating dissipation peaks in the southern auroral zone, they did not appear to be very effective in generating TIDs. This is probably due to the larger dissipative effects by ion drag in the sun-lit Southern Hemisphere [*Emery et al.*, 1999; *Buonsanto et al.*, 1999].

Figure 5b illustrates the variations of h_mF_2, which denotes the height of the F layer electron density peak. Enhanced southward winds modulated by TIDs lifted the F layer in the Northern Hemisphere and lowered it in the Southern Hemisphere, with the demarcation lying at ~10°S which corresponds roughly to the geomagnetic equator at 70°W.

The corresponding perturbations of the N_2/O ratio and f_oF_2 are shown in Figures 5c and 5d, respectively. Unlike the changes in h_mF_2, the changes in the N_2/O ratio do not seem to be significantly affected by TIDs. N_2/O increased in the regions above ~40°N and below ~50°S, with small decreases in between. In contrast, the variations in f_oF_2 were more complicated. Above ~40°N a positive storm phase of increased f_oF_2 was ev-

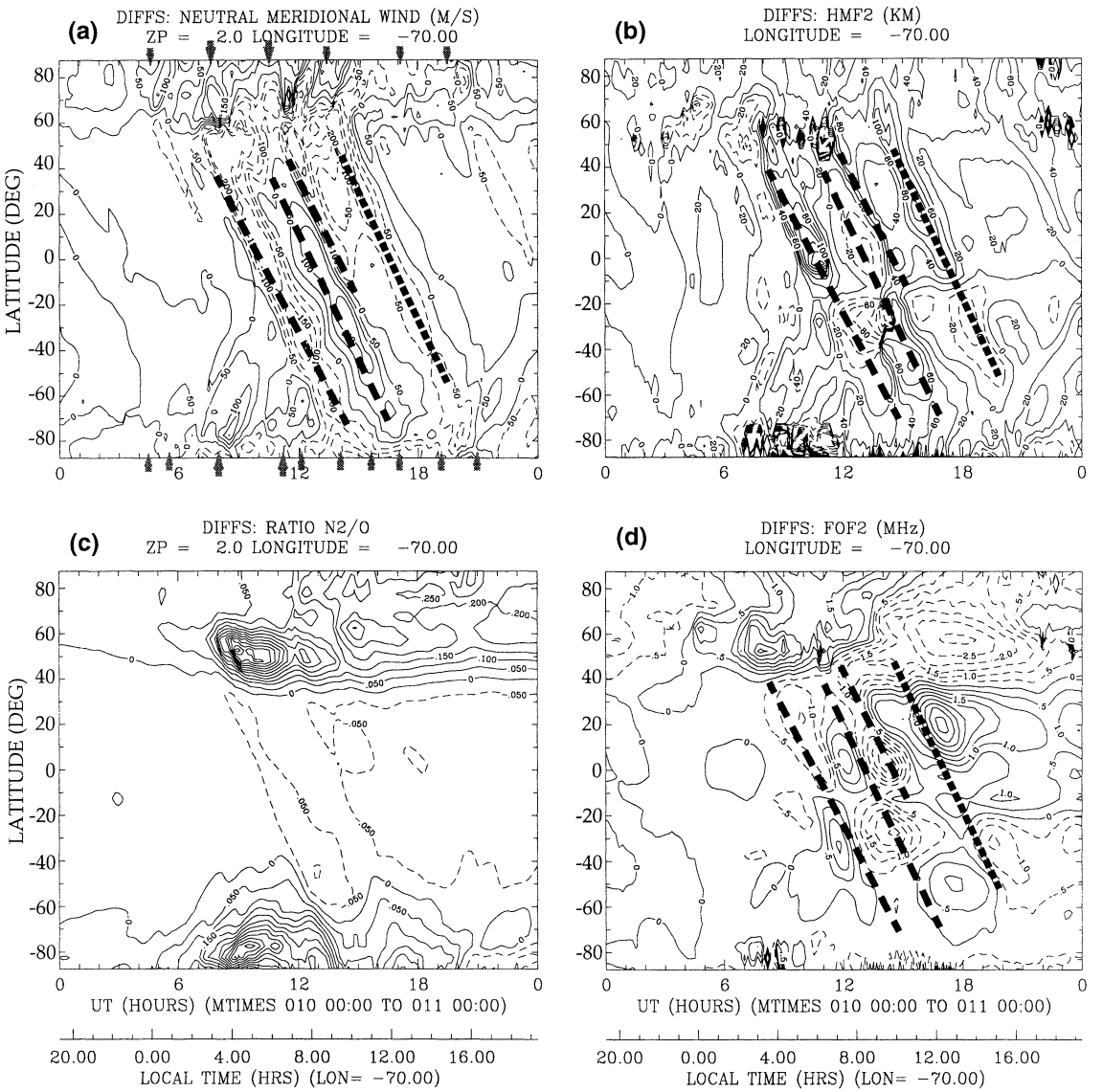

Figure 5. Difference plots of various fields at 70°W on January 10, 1997: (a) the difference neutral meridional wind at constant pressure level $ZP = 2$ (corresponding roughly to an altitude of 300 km). Solid contours represent northward wind and dashed contours equatorward wind; (b) the difference h_mF_2, with the solid and dashed contours representing the increase and decrease of h_mF_2; (c) the difference of the N_2/O ratio at $ZP = 2$, with the solid and dashed contours representing the increase and decrease in N_2/O; and (d) the difference f_oF_2, with the solid and dashed contours representing the increase and decrease of f_oF_2. The heavy dashed lines outline phase propagations of meridional wind, h_mF_2, and f_oF_2, where the long heavy dashed lines indicate a negative correlation between f_oF_2 and h_mF_2 and the short heavy dashed lines a positive correlation.

ident before 1300 UT but reversed to a negative storm phase afterward. This daytime f_oF_2 decrease is consistent with the negative storm phase observed by the Millstone Hill radar [*Mikhailov and Förster*, 1999]. At middle and low latitudes there were alternating positive and negative storm phases between ~0800 and 1500 UT, followed by a positive storm phase. Below ~50°S the storm had caused very little change in f_oF_2 (with a magnitude less than 1 MHz) along this longitude sector.

As demonstrated by Figures 5c and 5d, there is little direct anticorrelation between N_2/O and f_oF_2 changes along 70°W longitude prior to ~1300 UT (or ~9 LT). The increase of f_oF_2 in the northern auroral zone before 1300 UT was associated with enhanced auroral precipitation during the storm main phase despite the fact that N_2/O ratio was also increased simultaneously due to the enhancement of Joule heating that caused the atmospheric upwelling. After 1300 UT the storm as well as substorm activities subsided, and the increase in N_2/O was then seen to be related to the decrease in f_oF_2 in the northern high-latitude region. This again is consistent with the independent model calculation by *Mikhailov and Förster* [1999]. At midlatitudes and low

latitudes the increase and decrease in f_oF_2 appear to be inversely related to the changes in h_mF_2 between ~0800 and 1500 UT, as indicated by the long heavy dashed lines in Figures 5b and 5d. A positive correlation between f_oF_2 and h_mF_2, on the other hand, was found after ~1500 UT, about 4 hours into the storm recovery phase and when the associated longitudinal sector moved into the dayside; the most pronounced positive correlation is highlighted by the short heavy dashed lines.

3. Discussion

Strong latitudinal and longitudinal dependencies in storm response are rather evident in our model results, and they are further corroborated by the ionosonde observations. As illustrated in Figure 4, while North America experienced a negative storm phase, a strong positive storm phase formed in the Central American region. Positive storm phases were also produced in western Europe and over Russia. But the storm hardly affected the Asian region at all. As pointed out by *Prölss* [1993] and *Fuller-Rowell et al.* [1997], storm surges tend to develop in the night sector, where neutral winds are preferably equatorward, and in the longitudinal sector containing the magnetic pole. In the case under study, the storm commenced at ~0600 UT when the American sector was on the nightside. It therefore experienced the greatest magnetospheric forcing and ionospheric heating, resulting in the strongest storm effects in that sector. In contrast, the Asian sector was located on the dayside at the storm commencement and the storm effects there were almost negligible.

Composition changes in the middle-latitude region are one of the prominent storm features. Remote observations of far ultraviolet (FUV) dayglow by the DE 1 satellite have shown decreased brightness of FUV emissions following the onset of geomagnetic activity at high latitudes [*Craven et al.*, 1994; *Nicholas et al.*, 1997; *Immel et al.*, 1997], implying a reduction in the O/N_2 column concentrations [*Strickland et al.*, 1995]. Our simulation results are consistent with the composition changes as inferred from the FUV dayglow observations by showing the increase of the N_2/O ratio shortly after the storm commencement. An increase in N_2/O first evolved over the auroral zone, caused by the atmospheric upwelling due to enhanced Joule heating as well as particle heating. The N_2/O enhancement expanded to lower latitudes and was transported toward the dayside by corotation. Once on the dayside the N_2/O enhancement continued to persist even 10 hours into the storm recovery phase. The enhancement gradually diminished locally as vertical diffusion gradually restored equilibrium.

Although increases (decreases) in molecular density can cause negative (positive) storm phases, the overall storm effects are determined by several competing processes, such as auroral ionization enhancements, storm-induced circulation changes, and large-scale TADs/TIDs [*Rishbeth*, 1989; *Prölss et al.*, 1991; *Fuller-Rowell et al.*, 1997]. Equatorward winds tend to lift the ionization maximum height up into regions where neutral molecular densities are lower so recombination of electrons with ions becomes slower, generating positive storm effects [*Rishbeth*, 1989; *Prölss et al.*, 1991; *Prölss*, 1993; *Field et al.*, 1998; *Förster et al.*, 1999]. Poleward winds, conversely, can generate negative storm effects. A positive correlation between NmF_2 and h_mF_2 is therefore often anticipated. However, a strong anticorrelation between disturbances in NmF_2 and in h_mF_2 has also been reported, especially for variations with timescales of a few hours or less [e.g., *Wright*, 1961; *Shashun'kina*, 1966; *Testud and Vasseur*, 1969; *Harper*, 1972; *Park*, 1974; *Prölss and Jung*, 1978; *Deminova et al.*, 1998]. Modeling studies of large-scale TIDs produced by high-latitude disturbances have also shown an approximate anticorrelation between the variations of h_mF_2 and NmF_2, though with a lag of the maxima and minima of h_mF_2 behind the minima and maxima of NmF_2 [e.g., *Testud and Vasseur*, 1969; *Francis*, 1973; *Roble et al.*, 1978; *Prölss and Jung*, 1978; *Zevakina et al.*, 1978; *Fesen et al.*, 1989]. In these studies the meridional wind was important for raising and lowering the ionospheric layer, leading to ensuing maxima and minima in h_mF_2, while vertical shear of the meridional wind was important for compressing and expanding the layer, leading to ensuing maxima and minima in NmF_2. When the wind and the wind shear are the dominant influences on h_mF_2 and NmF_2, as opposed to the influences due to variations in production, loss, and diffusion, then the phase relation that exists between variations of h_mF_2 and NmF_2 is largely determined by the phase relation that exists between variations of the meridional wind velocity and the vertical shear of that velocity.

Our study shows an approximately negative correlation between f_oF_2 and h_mF_2 in the 70°W sector for large-scale TIDs during the storm main phase and its early recovery phase in the local morning sector of 04-10 LT. The long heavy dashed lines drawn in Figures 5a, 5b, and 5d illustrate the relationship amongst the meridional wind, h_mF_2 and f_oF_2. The southward (northward) wind surges raised h_mF_2 in the Northern (Southern) Hemisphere and lowered it in the opposite hemisphere, while at the same time, f_oF_2 tended to change oppositely to h_mF_2. During the late storm recovery phase under sunlit conditions, however, a positive correlation between f_oF_2 and h_mF_2 became evident (indicated by the short heavy dashed lines).

Figure 6 shows the variations of the meridional wind and electron density at 17.5°N and 70°W for the period of 0800-1800 UT on January 10. In Figure 6a the dashed and solid contours represent southward and northward winds, respectively, and the triangles indicate h_mF_2. Figure 6a clearly shows that southward winds lift h_mF_2, whereas northward winds tend to lower h_mF_2. Note that the onsets of h_mF_2 uplift (indicated by the upward arrows) occurred when the ver-

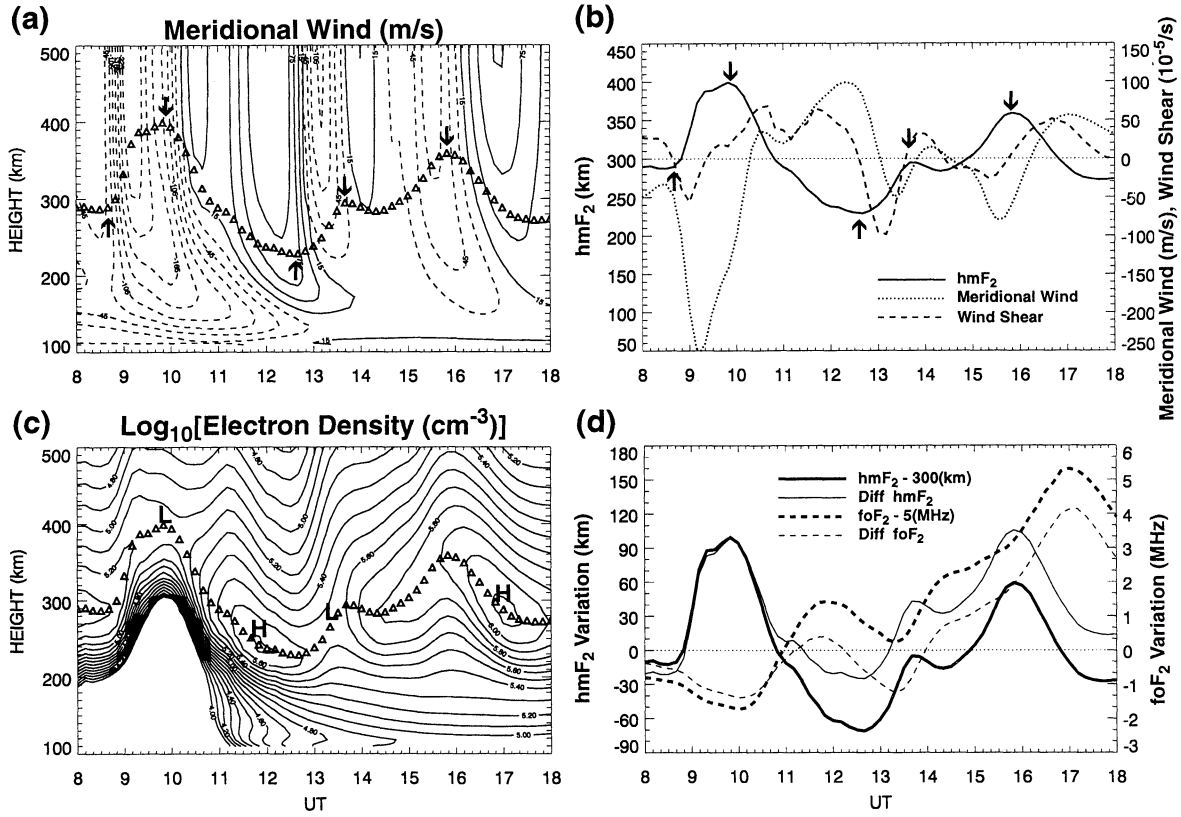

Figure 6. (a) Distributions of neutral meridional wind. (b) Variations of h_mF_2 (solid line), meridional wind (dotted line) and the vertical shear of meridional wind (dashed line). (c) Distributions of electron density. (d) Variations of the storm time h_mF_2 (thick solid line), the difference h_mF_2 (thick solid line), the storm time f_oF_2 (thick dashed line), and the difference f_oF_2 (thin dashed line). All panels cover the period between 0800 and 1800 UT on January 10, 1997, at 17.5°N and 70°W. The dashed and solid contours in Figure 6a represent southward and northward winds, respectively, and the upward and downward arrows indicate the onsets of h_mF_2 uplift and downfall. The triangles in both Figures 6a and 6c correspond to the height of h_mF_2. The letters L and H in Figure 6b denote the relative high and low electron densities at h_mF_2.

tical shear of the poleward wind was negative near the height of h_mF_2, namely, the meridional wind was more southward above h_mF_2 than below; whereas the onsets of subsidence (indicated by the downward arrows) occurred when the wind shear was positive, that is, the wind was more northward above h_mF_2 than below. The positive and negative wind shears contributed to the contraction and expansion of the F_2 layer.

The relation between the meridional wind at h_mF_2, the vertical shear of the meridional wind at h_mF_2, and h_mF_2 is shown in Figure 6b. Comparison of the solid line (h_mF_2) with the dotted line (northward meridional wind) shows an approximate anticorrelation between these two quantities. The arrows are similar to those shown in Figure 6a which indicate the rise and fall of h_mF_2. When h_mF_2 was decreasing (increasing), it is seen that the wind shear was generally positive (negative), and thus contributed to increasing (decreasing) NmF_2. Notice that the maxima (minima) in the wind shear generally preceded the maxima (minima) in the wind itself. This is a property of gravity waves that are propagating equatorward and upward out of the auroral zone, forming phase surfaces which are tilted equatorward toward higher altitudes.

Figure 6c shows the variations of electron density. The triangles indicate h_mF_2, and relative high and low NmF_2 values are indicated by the letters H and L, respectively. Using the continuity equation for electron density, we calculated that the fluctuating wind shear was usually a major contributor to the rate of change of NmF_2 (as opposed to fluctuations in loss, diffusion, and production), and tended to be the dominant contributor when the fluctuations were rapid and when h_mF_2 was neither very high nor low.

Figure 6d shows by thick solid and dashed lines the disturbed-time h_mF_2 and f_oF_2 values, and by thin solid and dashed lines the differences between the disturbed time and the quiet time background values as shown in Figures 5b and 5d at 17.5°N, respectively. It is noticed that the variations of difference h_mF_2 and f_oF_2 closely resemble those of disturbed-time h_mF_2 and f_oF_2. An approximate anticorrelation between h_mF_2 and f_oF_2 is present prior to 1500 UT between each corresponding pair of solid and dashed lines, and the minima (maxima)

in h_mF_2 tend to lag behind the corresponding maxima (minima) in f_oF_2 except during the first period of anticorrelation between 0900 and 1100 UT. This time lag is associated with the phase relation between the wind and the wind shear mentioned above. There are three distinct phases of anticorrelation: 0900-1100 UT, 1100-1300 UT, and 1300-1500 UT. They are coincident with the three periods marked by the long heavy dashed lines in Figures 5b and 5d. After ~1500 UT this longitude sector of 70°W had rotated into the daylight, and h_mF_2 became approximately positively correlated with f_oF_2 even though the wind shear was still present. The daytime positive correlation between h_mF_2 and f_oF_2 can be readily explained by the smaller recombination rate as h_mF_2 increases [*Rishbeth*, 1989; *Prölss et al.*, 1991; *Prölss*, 1993]. The time lag between f_oF_2 and h_mF_2 during this positive correlation phase (with the h_mF_2 maximum leading the f_oF_2 maximum by ~1 hour) is consistent with the calculated recombination rate of $\sim 2 \times 10^{-4}$ s^{-1}.

4. Summary

A numerical simulation was performed to investigate how the ionosphere and thermosphere respond to the geomagnetic storm of January 10, 1997. Using time-varying, realistic specifications of plasma convection and auroral precipitation from AMIE as inputs, the TIE-GCM simulation shows a complex storm response with strong latitudinal, longitudinal, and UT dependencies. Among the most pronounced storm features was the presence of opposite storm phases at middle and low latitudes.

The model simulation shows how TEC varies dynamically during the storm. Over the northern auroral zone there was an overwhelming TEC enhancement caused by direct ionization associated with enhanced auroral precipitation; an increase of 10 TECU in magnitude was found during the intervals of strong substorm activity. Storm time changes in O^+ flux at the upper boundary, which are not considered in the simulation, could significantly alter this prediction. At middle and low latitudes, TEC changes consisted of both TEC enhancement and depletion. Although TEC as derived from the TIE-GCM is actually the electron column density between 95 and ~600 km, changes in TEC were found to be closely related to changes of the F layer peak electron density. The enhancement and depletion of TEC were therefore the reflection of positive and negative storm phases.

Our simulation shows that the approximate anticorrelation between h_mF_2 and NmF_2 results from vertical transport of plasma by the gravity wave winds, even in the absence of horizontal transport by these winds (the TIE-GCM neglects the latter form of plasma transport). Such an anticorrelation has previously been interpreted as a result of storm-generated transequatorial winds which deplete electron concentrations in the upwind hemisphere and enhance them in the downwind hemisphere [*Fesen et al.*, 1989]. Although not shown in the paper, our calculation indicates that the vertical shear of meridional wind at the h_mF_2 height can account for much of the change in NmF_2.

This paper has demonstrated the complex nature of ionospheric storm effects owing to the interplay of several physical processes. Understanding how the ionosphere and thermosphere respond to geomagnetic storm remains a challenging task. The qualitative agreement in NmF_2 between the ionosonde observations and model simulations indicates that the TIE-GCM is able to correctly reproduce the observed positive and negative storm phases when the magnetospheric energy inputs are realistically specified. But the quantitative discrepancy with observations calls for further refinements of the model, for example, a more realistic plasma coupling with the magnetosphere.

Acknowledgments. We thank the community for providing various data that have been used in AMIE for this study. Most ionosonde data were provided by the National Geophysical Data Center in Boulder, and the Kokubunji ionosonde data were prepared by K. Igarashi at Communications Research Laboratory in Tokyo, Japan, for which we are grateful. NCAR is sponsored by National Science Foundation. This work was supported in part by the NASA Sun-Earth Connection Theory and Guest Investigator programs and by the NSF Space Weather program.

Janet G. Luhmann thanks both of the referees for their assistance in evaluating this paper.

References

Bilitza, D., International References Ionosphere 1990, NSSDC/WDC-A-R&S 90-22, Nat. Space Sci. Data Cent./ World Data Cent. A for Rockets and Satellites, Greenbelt, Md., Nov. 1990.

Buonsanto, M. J., S. A. Gonzalez, G. Lu, B. W. Reinisch, and J. P. Thayer, Coordinated incoherent radar study of the January 1997 storm, *J. Geophys. Res., 104*, 24,625-24,637, 1999.

Burns, A. G., T. L. Killeen, and R. G. Roble, A simulation of thermospheric composition changes during an impulsive storm, *J. Geophys. Res., 96*, 14,153-14,167, 1991.

Burns, A. G., T. L. Killeen, G. R. Carignan, and R. G. Roble, Large enhancements in the O/N_2 ratio in the evening sector of the winter hemisphere during geomagnetic storms, *J. Geophys. Res., 100*, 14,661-14,671, 1995.

Craven, J. D., A. C. Nicholas, L. A. Frank, D. J. Strickland, and T. J. Immel, Variation in the FUV dayglow after intense auroral activity, *Geophys. Res. Lett., 21*, 2793-2796, 1994.

Deminova, G. F., V. M. Shashunkina, and E. E. Goncharova, A global empirical model of effects of large-scale internal gravity waves in the night-time ionosphere, *J. Atmos. Sol. Terr. Phys., 60*, 227-245, 1998.

Emery, B. A., C. Lathuillere, P. G. Richards, R. G. Roble, M. J. Buonsanto, D. J. Knipp, P. Wilkinson, D. P. Sipler, and R. Niciejewski, Time dependent thermospheric neutral response to the 2-11 November 1993 storm period, *J. Atmos. Sol. Terr. Phys., 61*, 329-350, 1999.

Farrugia, C. J., et al. Geoeffectiveness of three Wind magnetic clouds: A comparative study, *J. Geophys. Res., 103*, 17,261-17,278, 1998.

Fesen, C. G., G. Crowley, and R. G. Roble, Ionospheric effects at low latitudes during the March 22, 1979, geomagnetic storm, *J. Geophys. Res., 94*, 5405-5417, 1989.

Fesen, C. G., R. G. Roble, and E. C. Ridley, Thermospheric tides at equinox: Simulations with coupled composition and auroral forcings, 2, Semidiurnal component, *J. Geophys. Res., 96*, 3663-3677, 1991.

Fesen, C. G., G. Crowley, R. G. Roble, A. D. Richmond, and B. G. Fejer, Simulation of the pre-reversal enhancement in the low-latitude vertical ion drifts, *Geophys. Res. Lett., 27*, 1851-1854, 2000.

Field, P. R., H. Rishbeth, R. J. Moffett, D. W. Idenden, T. J. Fuller-Rowell, G. H. Millward, and A. D. Aylward, Modelling composition changes in *F*-layer storm, *J. Atmos. Sol. Terr. Phys., 60*, 523-543, 1998.

Förster, M., A. A. Namgaladze, and R. Y. Yurik, Thermospheric composition changes deduced from geomagnetic storm modeling, *Geophys. Res. Lett., 26*, 2625-2628, 1999.

Fox, N. J., M. Peredo, and B. J. Thompson, Cradle to grave tracking of the January 6-11, 1997, Sun-Earth connection event, *Geophys. Res. Lett., 25*, 2461-2464, 1998.

Francis, S. H., Acoustic-gravity models and large-scale traveling ionospheric disturbances of a realistic, dissipative atmosphere, *J. Geophys. Res., 78*, 2278-2301, 1973.

Fuller-Rowell, T. J., M. V. Codrescu, R. J. Moffett, and S. Quegan, Response of the thermosphere and ionosphere to geomagnetic storms, *J. Geophys. Res., 99*, 3893-3914, 1994.

Fuller-Rowell, T. J., M. V. Codrescu, R. J. Moffett, and S. Quegan, On the seasonal response of the thermosphere and ionosphere to geomagnetic storms, *J. Geophys. Res., 101*, 2343-2353, 1996.

Fuller-Rowell, T. J., M. V. Codrescu, R. G. Roble, and A. D. Richmond, How does the thermosphere and ionosphere react to a geomagnetic storm? in *Magnetic Storms*, *Geophys. Monogr. Ser.*, vol. 98, edited by B. T. Tsurutani et al. pp. 203-225, AGU, Washington, D. C., 1997.

Gallagher, D. L., P. D. Craven, and R. H. Comfort, Global core plasma model, *J. Geophys. Res., 105*, 18,819-18,833, 2000.

Harper, R. M., Observations of a large nighttime gravity wave at Arecibo, *J. Geophys. Res., 77*, 1311-1315, 1972.

Immel, T. J., J. D. Craven, and L. A. Frank, Influence of IMF *By* on large-scale decreases in O column density at middle latitudes, *J. Atmos. Terr. Phys., 59*, 725-737, 1997.

Lu, G., et al. Global energy deposition during the January 1997 magnetic cloud event, *J. Geophys. Res.*, 103, 11,685-11,694, 1998a.

Lu, G., X. Pi, A. D. Richmond, and R. G. Roble, Variations of total electron content during geomagnetic disturbances: A model/observation comparison, *Geophys. Res. Lett., 25*, 253-256, 1998b.

Mikhailov, A. V., and M. Förster, Some F2-layer effects during the January 06-11, 1997 CEDAR storm period as observed with the Millstone Hill incoherent scatter facility, *J. Atmos. Sol. Terr. Phys., 61*, 249-261, 1999.

Nicholas, A. C., J. D. Craven, and L. A. Frank, A survey of large-scale variations in thermospheric oxygen column density with magnetic activity as inferred from observation of the FUV dayglow, *J. Geophys. Res., 102*, 4493-4510, 1997.

Park, C. G., A morphological study of substorm-associated disturbances in the ionosphere, *J. Geophys. Res., 79*, 2821-2827, 1974.

Prölss, G. W., Seasonal variation of atmospheric-ionospheric disturbances, *J. Geophys. Res., 82*, 1635-1640, 1977.

Prölss, G. W., Storm-induced changes in the thermospheric composition at middle latitudes, *Planet. Space Sci., 35*, 807-811, 1987.

Prölss, G. W., On explaining the local time variation of ionospheric storm effects, *Ann. Geophys., 11*, 1-9, 1993.

Prölss, G. W., and M. J. Jung, Travelling atmospheric disturbances as a possible explanation for daytime positive storm effects of moderate duration at middle latitudes, *J. Atmos. Terr. Phys., 40*, 1351-1354, 1978.

Prölss, G. W., L. H. Brace, H. G. Mayr, G. R. Carignan, T. L. Killeen, and J. A. Klobuchar, Ionospheric storm effects at subauroral latitudes: A case study, *J. Geophys. Res., 96*, 1275-1288, 1991.

Richmond, A. D., and Y. Kamide, Mapping electrodynamic features of the high-latitude ionosphere from localized observations: Technique, *J. Geophys. Res., 93*, 5741-5759, 1988.

Richmond, A. D., E. C. Ridley, and R. G. Roble, A thermosphere/ionosphere general circulation model with coupled electrodynamics, *Geophys. Res. Lett., 19*, 601-604, 1992.

Rishbeth, H., *F*-region storms and thermospheric circulation, in *Electromagnetic Coupling in the Polar Clefts and Caps*, edited by P. E. Sandholt and A. Egeland, pp. 393-406, Kluwer Acad., Norwell, Mass., 1989.

Rishbeth, H., T. J. Fuller-Rowell, and D. Rees, Diffusive equilibrium and vertical motion in the thermosphere during a sever magnetic storm: A computational study, *Planet. Space Sci., 35*, 1157-1165, 1987.

Roble, R. G., A. D. Richmond, W. L. Oliver, and R. M. Harper, Ionospheric effects of the gravity wave launched by the September 18, 1974, sudden commencement, *J. Geophys. Res., 83*, 999-1009, 1978.

Roble, R. G., J. M. Forbes, and F. A. Marcos, Thermospheric dynamics during the March 22, 1979, magnetic storm, 1, Model simulation, *J. Geophys. Res., 92*, 6045-6068, 1987.

Rodger, A. S., G. L. Wrenn, and H. Rishbeth, Geomagnetic storms in the Antarctic *F* region, II, Physical interpretation, *J. Atmos. Terr. Phys., 51*, 851-866, 1989.

Sanchez, E. R., J. P. Thayer, J. D. Kelly, and R. A. Doe, Energy transfer between the ionosphere and magnetosphere during the January 1997 CME event, *Geophys. Res. Lett., 25*, 2597-2600, 1998.

Schlegel, K., and P. N. Collis, The storm of 10 January 1997: Electrodynamics of the high-latitude *E* region from EISCAT data, *J. Atmos. Sol. Terr. Phys., 61*, 217-222, 1999.

Shashun'kina, V. M., Ionospheric effects of the sudden commencement of the magnetic storm of July 15, 1959, *Geomagn. Aeron.*, Engl. Transl., *6*, 111-114, 1966.

Strickland, D. J., J. S. Evans, and L. J. Paxton, Satellite remote-sensing of thermospheric O/N_2 and solar EUV, *J. Geophys. Res., 100*, 12,217-12,226, 1995.

Testud, J., and G. Vasseur, Ondes de gravité dans la thermosphère, *Ann. Géophys., 25*, 525-546, 1969.

Wright, M. D., Possible identification of atmospheric waves associated with ionospheric storms, *Nature, 190*, 898-899, 1961.

Zevakina, R. A., A. A. Namgaladze, and V. M. Smertin, Interpretation of positive disturbances of the F_2 region, *Geomagn. Aeron.*, Engl. Transl., *18*, 708-710, 1978.

B. A. Emery, G. Lu, A. D. Richmond, and R. G. Roble, High Altitude Observatory, NCAR, 3450 Mitchell Lane, Boulder, CO 80301, USA. (emery@ucar.edu; ganglu@ucar.edu; richmond@ucar.edu; roble@ucar.edu)

(Received January 4, 2001; revised April 6, 2001; accepted April 12, 2001.)